Influence of Three Dimensionality on Propulsive Flapping

A. N. Zurman-Nasution[1]†, B. Ganapathisubramani and G. D. Weymouth

Faculty of Engineering and Environment, University of Southampton, University Road, Southampton SO17 1BJ, UK

(Received xx; revised xx; accepted xx)

Propulsive flapping foils are widely studied in the development of swimming and flying animal-like autonomous systems. Numerical studies in this topic are mainly two-dimensional (2D) studies as they are quicker and cheaper, but, this inhibits the three-dimensional (3D) evolution of the shed vortices from leading- and trailing-edges. In this work, we examine the similarities and differences between 2D and 3D simulations through a case study in order to evaluate the efficacy and limitations of using 2D simulations to describe a 3D system. We simulate an infinite-span NACA0016 foil both in 2D and 3D at a Reynolds number of 5300 and an angle-of-attack of 10°. The foil is subject to prescribed heaving and pitching kinematics with varying trailing-edge deflection amplitude A. Our primary finding is that the flow and forces are effectively 2D at *intermediate* amplitude-based Strouhal numbers ($St_A = 2Af/U$ where U is the freestream velocity and f is the flapping frequency); $St_A \approx 0.3$ for heaving, $St_A \approx 0.3$–0.6 for pitching and $St_A \approx 0.15$–0.45 for coupled motion, while 3D effects dominate outside of these ranges. These 2D regions begin when the fluid energy induced by the flapping motion overcomes the 3D vortex shedding found on a stationary foil, and the flow reverts back to 3D when the strength of the shed vortices overwhelms the stabilizing influence of viscous dissipation. These results indicate that 3D-to-2D transitions or vice-versa are a balance between the strength and stability of leading-/trailing-edge vortices and the flapping energy. 2D simulations can still be used for flapping flight/swimming studies provided the flapping amplitude/frequency is within a given range.

Key words: –

1. Introduction

Engineering applications such as MAVs (micro air vehicles) and energy harvesting are designed to mimic the propulsive flapping mechanism of swimming and flying animals although these applications are less efficient. The early research on propulsive flapping of swimming animals by Triantafyllou *et al.* (1991, 1993) set a range for effective Strouhal numbers ($St_A = 2Af/U$, where A is the trailing-edge amplitude, f is the flapping frequency and U is the freestream velocity) as 0.25–0.35, but it was argued only for large aspect-ratio (AR) tails (Eloy 2012; Rohr & Fish 2004). Nevertheless, flapping foil research primarily focus on $St_A = 0.2$–0.4 as proven by experiments where interesting transitions exist, i.e drag–thrust transition and wake transition from Bénard-von-Kármán (drag-

† Email address for correspondence: A.N.Zurman-Nasution@soton.ac.uk

producing) to reverse Bénard-von-Kármán (thrust-producing) vortex street (Andersen *et al.* 2016; Godoy-Diana *et al.* 2008).

The majority of numerical studies for flapping foil are mostly in 2D—due to its simplicity and cost savings—and have shown consistency with experiments. Kooches-fahani (1989) indicated that the flow at certain range of St_A over a high AR foil, which experiences periodical 2D motions such as pure heaving and pure pitching, is mostly assumed to be 2D. Researchers found that soap film experiments agreed with 2D simulations (Andersen *et al.* 2016; Schnipper *et al.* 2009; Zhang 2017), and high AR foil experiments agreed with 2D simulations (Moriche *et al.* 2016; Muscutt *et al.* 2017). These studies, however, did not explain why the flapping foil being subjected to periodic high angles of attack remains two-dimensional while a stationary foil at the same (or similar) angles of attack experiences strong separation (Uddin *et al.* 2017) where 3D effects are not negligible.

Despite experiments using high AR foils to ensure 2D flow, three-dimensional effects should not be ruled out. Apart from tip vortices, the effect of leading-edge vortices (LEVs) has been shown to be important for high AR rotating wings (Fu *et al.* 2015; Lu *et al.* 2006; Carr *et al.* 2013). These vortices are the major contributors for force evolutions in flapping foil especially along the span because LEVs stabilise the spanwise force-variations (Triantafyllou *et al.* 2004) but only at low Rossby ($Ro = R/c$, where R is wingtip radius and c is mean chord length) as stated by Lentink & Dickinson (2009). At higher Ro, the LEVs are unstable due to Coriolis acceleration creating spanwise instability which is also predicted by Williamson (2006) for flow over a circular cylinder. These 3D effects have consequences on the 2D assumption for predictions, especially in spanwise force-fluctuations and would lead to inaccuracies in global parameters and local flow fields (Lei *et al.* 2001; Garcia *et al.* 2017), delayed and shortened recirculation area causing very low base pressures and over-predicted mean drag and lift-coefficient fluctuations (Mittal & Balachandar 1995).

In very recent work, the appearance of 2D to 3D transition in flow structures was observed by Deng *et al.* (2016). This was based on linear Floquet stability without any comprehensive 3D simulations thereby making the source/regime of this transition uncertain. In this work, this 2D to 3D transition is investigated using comprehensive 2D and 3D simulations across the range of flapping kinematics, including the analysis of average and fluctuating force-coefficients, vorticity metrics and energy distribution. The results demonstrate the limitations of strip theory and the parameter space where there is a need for full 3D simulations to examine propulsive flapping mechanisms of animals and animal-like like autonomous systems.

2. Methodology

The foil used in this research is NACA0016 with thickness $D = 0.16c$, where c is the chord length. The foil is placed in uniform flow with constant inflow speed U and fluid density ρ. The Reynolds number of $Re = Uc/\nu = 5300$ was chosen in order to be in the middle of Reynolds number regime of flapping flyers and swimmers ($1000 < Re < 10000$). Moreover, this Reynolds number also corresponds to the shear-layer transition regime of Williamson (1996). Finally, the simulations at higher Reynolds numbers ($Re \approx 10600$) for a limited number of cases did not change the conclusions reached in the following sections.

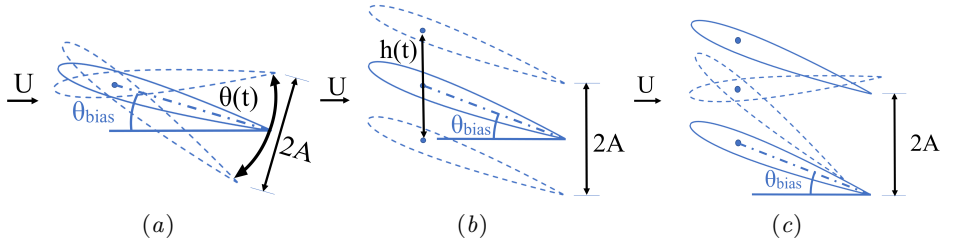

Figure 1: Kinematics with bias angle-of-attack, (a) pitching, (b) heaving and (c) coupled motions.

2.1. *Kinematics*

The governing kinematic parameter is the amplitude-based Strouhal number $St_A = St_D \cdot A_D$. In order to isolate the amplitude and frequency, we use

$$St_D = \frac{Df}{U} \qquad A_D = \frac{2A}{D} \tag{2.1}$$

where St_D is the thickness-based Strouhal number, A_D is the thickness-based amplitude, f is the frequency of flapping (in Hz) and the double amplitude $2A$ is measured at the trailing edge.

The foils are prescribed to undergo pure heave h, pure pitch θ and coupled pitch and heave. The motions are harmonic, with functional form

$$h(t) = A\sin(2\pi ft) \tag{2.2}$$

$$\theta(t) = \theta_0 \sin(2\pi ft + \psi) + \theta_{\text{bias}} \tag{2.3}$$

$$\theta_0 = \sin^{-1}\left(A/(0.75c)\right) \tag{2.4}$$

The pivot point for pitching motion is $0.25c$ from the leading edge. The coupled motion has a phase angle $\psi = 90°$, which was found as the most effective for propulsive flapping (Isogai *et al.* 1999). Due to this phase angle, pitching lags behind heaving for a quarter of a cycle causing it to be at minimum $\theta(t)$ when heaving has reached maximum $h(t)$. A bias angle-of-attack is employed to focus on lift-producing propulsive motion used mainly by bio-flyers, although some swimming animals were also reported to benefit from lift e.g. shark's pectoral fins. The bias angle-of-attack is fixed at $\theta_{\text{bias}} = 10° = \pi/18$ rad. This $10°$ angle is chosen because it sufficiently induces unsteadiness to the flow for stationary foil case.

In this work, we vary St_A by discretely increasing the amplitude from $A_D = 0.0625$–3.75 but keeping the frequency fixed at $St_D = 0.3$ following one vertical line in St_D-versus-A_D map of Andersen *et al.* (2016). This frequency is slightly above the stationary-foil vortex shedding frequency.

2.2. *Measurement metrics*

Results are presented based on thrust- (C_t) and lift- (C_l) force coefficients as follows:

$$C_t = -\frac{F_x}{0.5\rho SU^2} \qquad C_l = \frac{F_y}{0.5\rho SU^2} \tag{2.5}$$

where measured thrust force $(-F_x)$ and lift force (F_y) are calculated from the integration of pressure and viscous forces over the foil and S is the foil planform area. The mean, variance and power-spectral-density analysis of force-coefficient time-histories are used to highlight the differences across different kinematics.

$c/\Delta x$	$\overline{C_t}(3D)$	ϵ (3D)	$\overline{C_t}(2D)$	ϵ (2D)
48	0.884	36.7%	0.883	38.7%
64	0.965	30.9%	0.966	32.9%
128	1.342	3.9%	1.344	6.6%
256	1.397	—	1.44	—

Table 1: Grid convergence statistics for 3D and 2D simulations of a coupled motion case at $Re = 5300$, $A_D = 1.5$, and $\theta_{bias} = 0$. ϵ is relative error to $c/\Delta x = 256$.

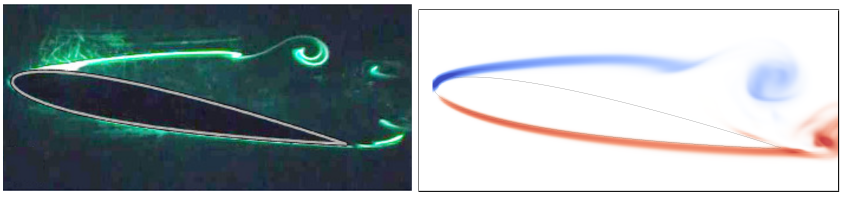

Figure 2: Accuracy comparison for instability starting-location of stationary NACA0012 at $Re = 5300$ and angle of attack 10°, (a) LIF flow visualisation of Wang *et al.* (2014), mean drag-coefficient $C_d = 0.14$, and (b) spanwise-vorticity of 3D simulation, $C_d = 0.133$. The instability starts at the first vortex roll-up.

2.3. *Computational method*

The computational package used for this research is Boundary Data Immersion Method (BDIM). Weymouth & Yue (2011) introduced BDIM using a robust and efficient Cartesian grid with implicit LES (iLES) solver. BDIM uses analytic meta-equations for immersed body in multi-phase flow with a smoothed interface domain using an integral kernel. BDIM has been validated, proved suitable for moving bodies and capable of resolving the flow at $Re = 10^5$ within 5% error for thrust prediction (Maertens & Weymouth 2014) .

For computational consistency between 2D and 3D simulations, the 3D grids are the spanwise extrusion of 2D grids and both simulations use the same iLES solver. Periodic boundary conditions are enforced along the spanwise direction of the foil and a span length of $6c$ is used for 3D simulation. The verification of grid convergence for 2D and 3D were carried out at $Re = 5300$ to identify the appropriate grid required. Table. 1 shows a comparison of the time-averaged thrust coefficient for different resolutions. It is seen that at a resolution of $c/\Delta x = 128$, the force coefficient converges to within 7% of the finer simulations (in both 2D and 3D). As a balance between the grid resolution and the number of simulations, a resolution of $c/\Delta x = 128$ is deemed sufficient to captures the dynamics of the flow and the parametric study in the following sections were carried out at this resolution but at a higher Reynolds number. A 3D simulation for a stationary NACA0012 is compared with the experiment result of Wang *et al.* (2014) in figure 2 showing an accurate instability location, and the drag coefficient is within 5%.

3. Comparison between 2D and 3D simulations

The two- and three-dimensional simulations are further compared based on the vortex-structure evolution, mean force-coefficients ($\overline{C_t}$ and $\overline{C_l}$), phase-averaged spanwise component of vorticity and fluctuations of force-coefficient signals.

3.1. *Overview and flow structures*

Figure 3 shows the variation of $\overline{C_t}$ with St_A for 2D and 3D simulations across three different kinematics (heave, pitch and coupled motions). The inset in the figures also show iso-surfaces of spanwise vorticity (ω_z) for a few selected cases (the cases as indicated with arrows in the figure). Starting at the lowest A_D (the lowest St_A), the flow structures appear to be three-dimensional with strong separation on the foil suction-side similar to a stationary foil. The values of $\overline{C_t}$ for both 2D and 3D simulations appear to be very similar to the $\overline{C_t}$ of a stationary-foil with the small discrepancy between 2D and 3D simulations.

With a slight increase in amplitude, the flow structures appear to be more coherent and become more two-dimensional. The $\overline{C_t}$ of 2D and 3D simulations now collapse to the same value(s). These 2D structures are found to persist until around $A_D = 1$ or $St_A = 0.3$ in all three types of motion. The beginning of 2D flow structures is accompanied by propulsive wakes evolving to reverse Bénard-von-Kármán in coupled motion or to asymmetric/deflected in heave and pitch. When A_D increases even higher, the 3D flow structures reappear eliminating the uniform 2D structures. They are followed by a substantial discrepancy in $\overline{C_t}$ between 2D and 3D simulations. The vortices appear to breakdown along the spanwise direction in the wake and this breakdown starts to creep up to the trailing-edge with increasing amplitude, which is consistent with the observations of Moriche *et al.* (2016). The flow structures at the trailing-edge are more "chaotic" along the spanwise direction, while the leading-edge vortices are relatively coherent along the span even at higher A_D.

The appearance of uniform 2D structures in all three types of motion shows that 2D simulations would indeed be sufficient over a certain range of Strouhal numbers, but the ranges are not the same for the three types of motion. The range is very limited for heaving motion, while the range is very similar for both pitching and coupled motions but the transition to 3D is earlier for the coupled motion. The similarity between pitching and coupled motion is understandable as the coupled motion is dominated by pitch motion in these current simulations. A heave dominant coupled motion would lead to the breakdown of 2D structures earlier and the range would be more similar to heaving-only motions.

3.2. *Effect of spanwise domain size*

In order to isolate the effect of spanwise domain size of the 3D simulations on the above observed results, a series of simulations with different spanwise lengths were carried out. All the simulations were confined at one kinematics: coupled motion at $A_D = 0.25$ where 3D structures begin to re-organise into 2D structures. Figure 4 shows that even when the span is reduced at $0.75c$, the $\overline{C_t}$ and C_t variance are almost constant and the 3D structures remain significant. This signifies the importance of the three-dimensionality of the spanwise vortices. This also suggests that a small spanwise domain length might be sufficient to capture the 3D effects provided the kinematics are in a certain range of amplitudes and frequencies.

3.3. *Statistics of thrust coefficient*

Along with the appearance of uniform 2D structures, the statistics of force coefficients (C_t and C_l) i.e. average, maximum, minimum and variance are similar for both 2D and 3D simulations. At lower and higher A_D when 3D structures appear, the force coefficients in 2D simulation exhibit very high levels of fluctuations. Similar force-coefficient fluctuations are shown for 2D simulation by Taira & Colonius (2009) for stationary flat-plates at a higher angle of attack.

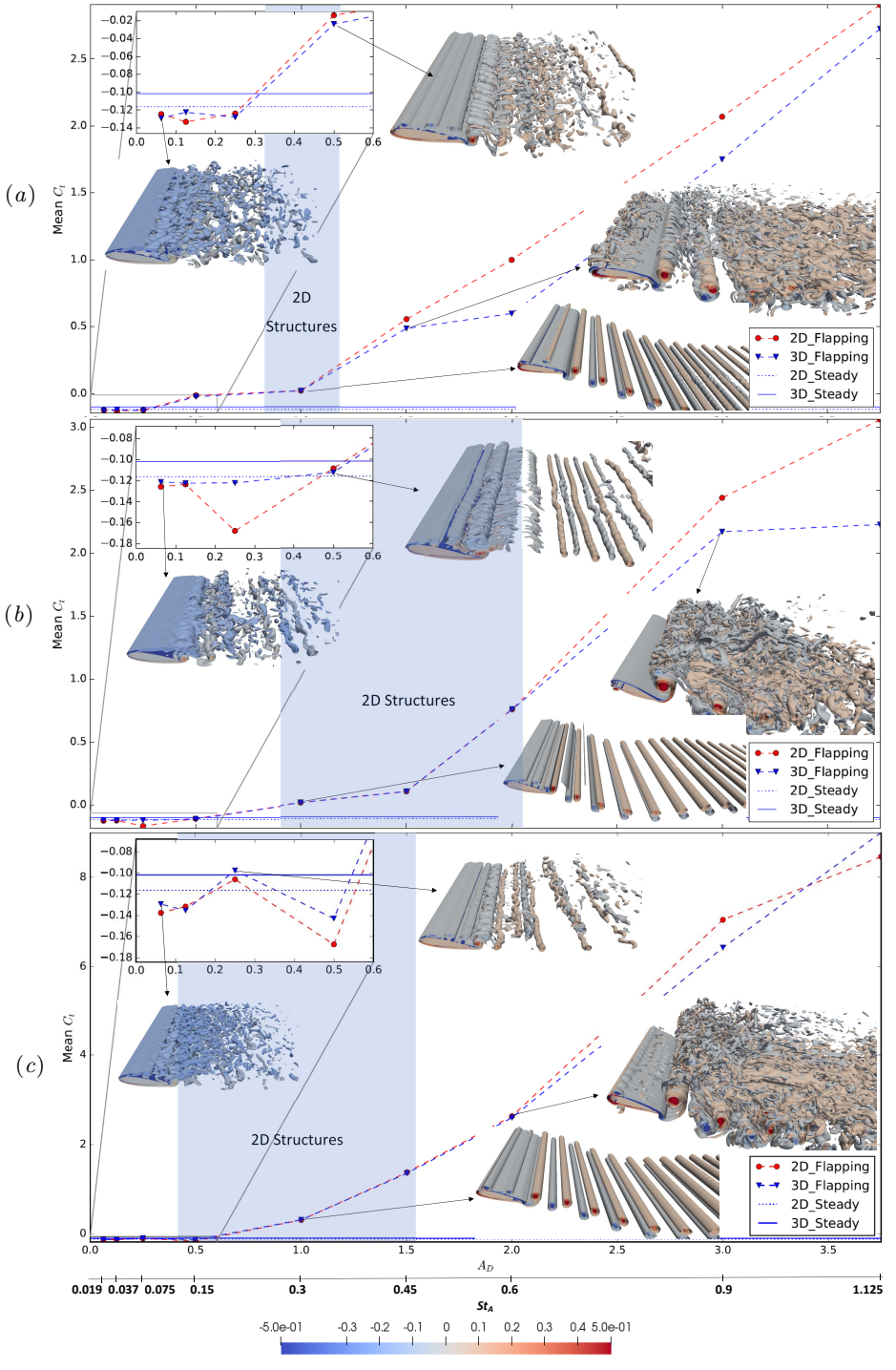

Figure 3: 3D iso-surfaces of ω_z on mean thrust-coefficient $\overline{C_t}$ versus trailing-edge amplitude A_D graph showing structure transitions at (a) heaving, (b) and pitching (c) coupled motions. Shaded areas locate 2D structures and non-shaded for 3D structures.

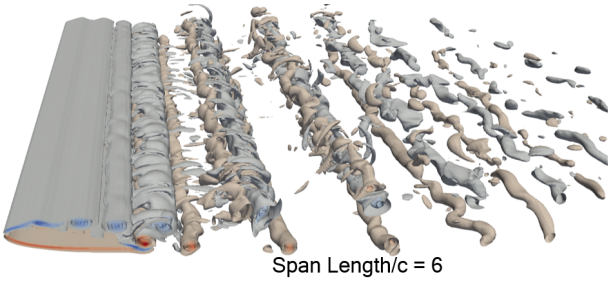

Span Length/c	$\overline{C_t}$	C_t Variance
6	-0.098	0.195
3	-0.1	0.197
1.5	-0.101	0.196
0.75	-0.1	0.196

Figure 4: Convergence of $\overline{C_t}$ and C_t variance with reduction in spanwise domain.

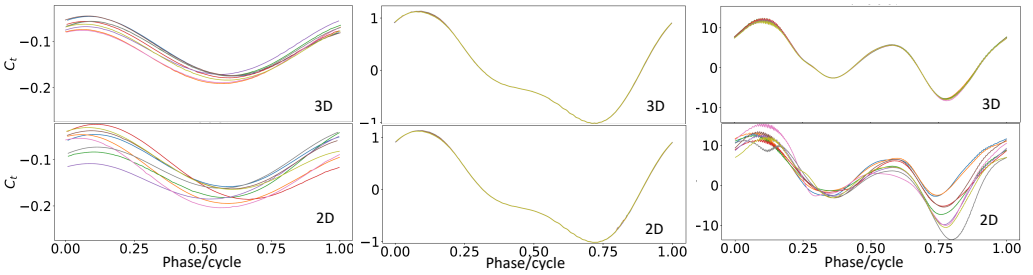

(a) (b) (c)

Figure 5: C_t comparison between 2D and 3D simulations of pitching motion for ten-cycles at (a) $A_D = 0.0625$, (b) $A_D = 1$ and (c) $A_D = 3.75$.

Figure 5 presents the comparison of C_t evolution for both 2D and 3D simulation for pitching motion. The tendency of C_t evolution for heaving and coupled motion are similar (not presented here for brevity). It can be seen that the 2D simulations exhibit cycle-to-cycle variations at lower and higher A_D while these variations are minimal for the intermediate amplitude. The cycle-to-cycle variations for the 3D simulations are weaker and only apparent for the low amplitude case. It was also found that both 2D and 3D simulations converged faster for the intermediate amplitude since the variations in the flow and the forces are minimal.

3.4. *Spanwise vorticity*

The instantaneous ω_z and the phase-averaged ω_z for 2D and 3D simulations are compared in Figure 6. For the 3D simulations, the vorticity is first spanwise-averaged prior to comparing it with 2D simulations. The presented figures are the cases where 3D structures appear at the lowest and the highest A_D in coupled motion. These are representative and similar features are observed in other kinematics as well.

As seen in figure 6(a) for a flapping amplitude of $A_D = 3.75$, the instantaneous cases for 2D and 3D simulations differ mainly in the wakes. The wakes in 2D simulation appear to be aperiodic and perhaps more chaotic. Meanwhile, the span-averaged vorticity in 3D simulations appears "cleaner" and more converged, making phase-averaging easier. This is because, in 3D simulations, the effect of spanwise averaging eliminates small perturbations in ω_z structure. However, in 2D simulations, this is not possible. Any small variation is exacerbated since there is no smoothing process and leads to the appearance of a chaotic wake.

In phase-averaged coupled motion (similar to other kinematics), the LEVs appear to be slightly smaller for 2D simulations compared to 3D simulations due to "jitter" in

the position of these vortices over different cycles. On the other hand, both types of simulations preserve one vortex pair behind the trailing edge. In the "far" wake, 2D simulations are chaotic since the vortices are strong and their self-induced motions alter the trajectories of the wake. Moreover, there are no mechanisms that can reduce the strength of these vortices (other than viscosity) and therefore they remain strong for an extended length/time. For the 3D simulations, the spanwise length provides a route for the transport of vorticity from the vortex core, thereby weakening the wakes downstream.

At the lowest A_D in figure 6(b), the difference between 2D and 3D simulations are not only in the wakes but also in the separation and recirculation areas. Similar to high A_D, the wakes for instantaneous 3D simulation have the spanwise direction to transport/diffuse vorticity compared to 2D simulations. Nonetheless, the wake widths of phase-averaged 2D and 3D simulations are similar. This perhaps explains why the difference in values of $\overline{C_t}$ in 2D and 3D simulations at lower A_D is relatively small. At lower A_D, the LEVs in both 2D and 3D simulations look similar but the trailing-edge vortices (TEVs) are different due to recirculation and flow inside the separation region. The vortices in 2D simulations at the separation region oscillate back and forth, while in 3D simulations they are more stable (see supplementary video). This oscillation appears at a lower frequency than the shedding frequency, which explains the appearance of additional low-frequency energy content in 2D simulation (see next section).

3.5. *Fourier analysis of force time-histories*

The power spectral density for the thrust coefficient time history is computed and plotted against frequencies normalised by the flapping frequency in figure 7(a). The peak frequency at $\tilde{f} = 1$ shows the flapping frequency. The ordinate is pre-multiplied by the frequency and presented in linear scale to ensure that equal areas under the curve represent equal "energy". The term energy here is used to represent the strength of the fluctuations in the signal. In fact, it should be noted that the total area under the curve is equal to the variance of C_t signal. Furthermore, the fluctuations can be categorised into three main regimes: $\tilde{f} < 1$ (low frequency), $\tilde{f} = 1$ (exactly at the flapping frequency) and $\tilde{f} > 1$ (high frequency). The integral of the area under the curve within these regimes provide the contributions from each of these regimes to the overall fluctuations.

Figure 7(b) shows a bar chart that compares the energy in force fluctuations from 2D simulations to their 3D counterparts. The total variance from the 3D simulations is taken as the reference to calculate percentages and this numerical value is indicated at the top of the bars. Consequently, the bars for the 2D simulations are sometimes higher than 100% since the variance in 2D is higher than 3D simulations. The contributions of three regimes to these fluctuations are shown in three colours as marked in figure 7(a). Different bars are shown for different kinematics and flapping amplitudes. Two bars on the left are also shown for the stationary foil where the total energy of 2D simulation is 8 times higher than the 3D value. However, the absolute values of these fluctuations are orders of magnitude smaller than the flapping motions as seen from the numerical value on the top of the bars.

It is clear from figure 7 that the appearance of coherent 2D structures is accompanied by a very similar distribution of fluctuations in the three different regimes in 2D and 3D simulations. Meanwhile, the appearance of 3D structures (spanwise variations) is accompanied by the discrepancy of force-fluctuation variance between 2D and 3D simulations where 2D simulation tends to exaggerate the levels of force fluctuations. Pitching has the lowest total energy among the three types of motion due to the nature of its kinematics, while pure heaving motion produces the largest levels of fluctuations. Meanwhile, coupled

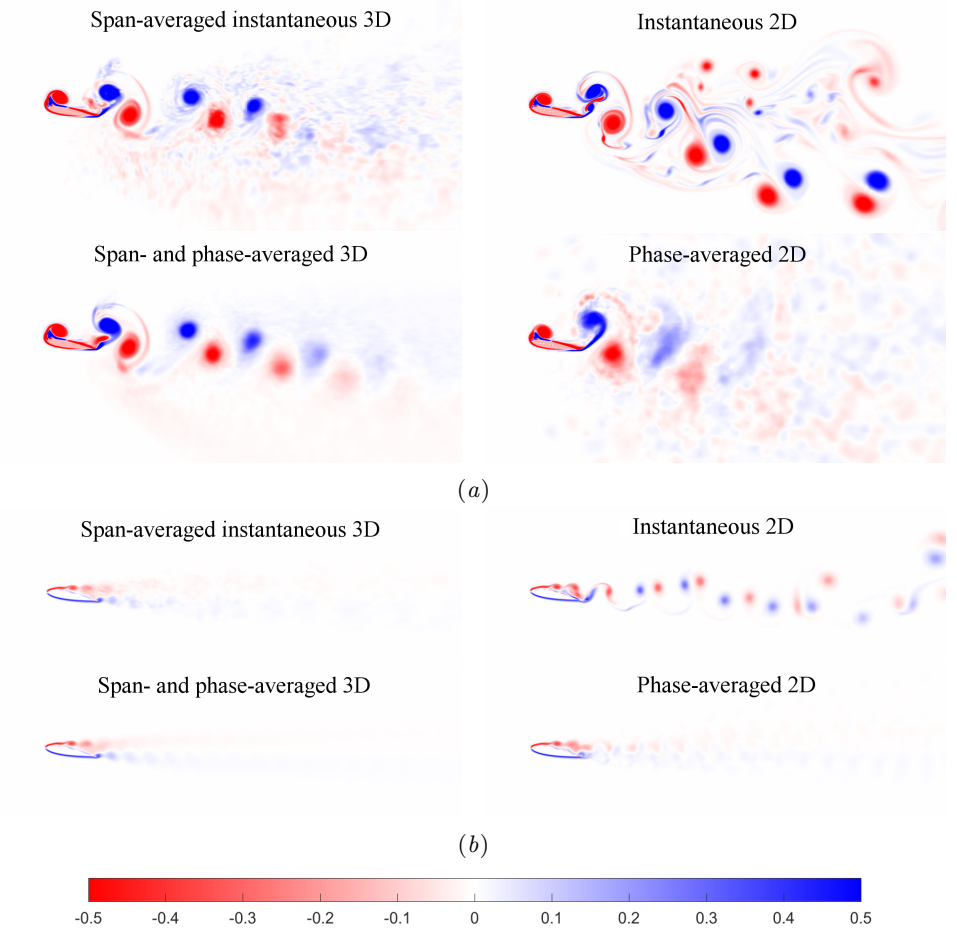

Figure 6: Instantaneous and phase averaged ω_z for coupled motion at (a) $A_D = 3.75$ and (b) $A_D = 0.0625$. The 3D simulations have been span-averaged prior to phase-average. Videos are provided.

motion energy is slightly lower than heaving because of 90° phase-lag between pitching and heaving parts of the motion.

The vortex shedding frequency of a stationary foil also appears in the flapping foil (as a low frequency) and can be seen to contribute to force fluctuations for low values of A_D. However, 2D simulations exhibit other additional low frequencies, which is stems from cycle-to-cycle variations as discussed in the previous section. As A_D increases, the energy from kinematics far exceeds the energy from vortex shedding. This explains the transition from 3D to 2D uniform structures. The energy from kinematics arranges the flow structures into uniform, reattaching separation zone so that the vortices move consistently from the leading-edge until detachment at the trailing-edge, leading to more organised downstream wakes. At higher values of A_D, higher harmonic frequencies start to appear and these make a contribution to the force fluctuations. The contributions from these higher frequencies are significantly higher in 2D simulations compared to 3D simulations since there are additional higher frequencies due to the appearance/movement of chaotic vortices as seen in figure 6 and figure 5.

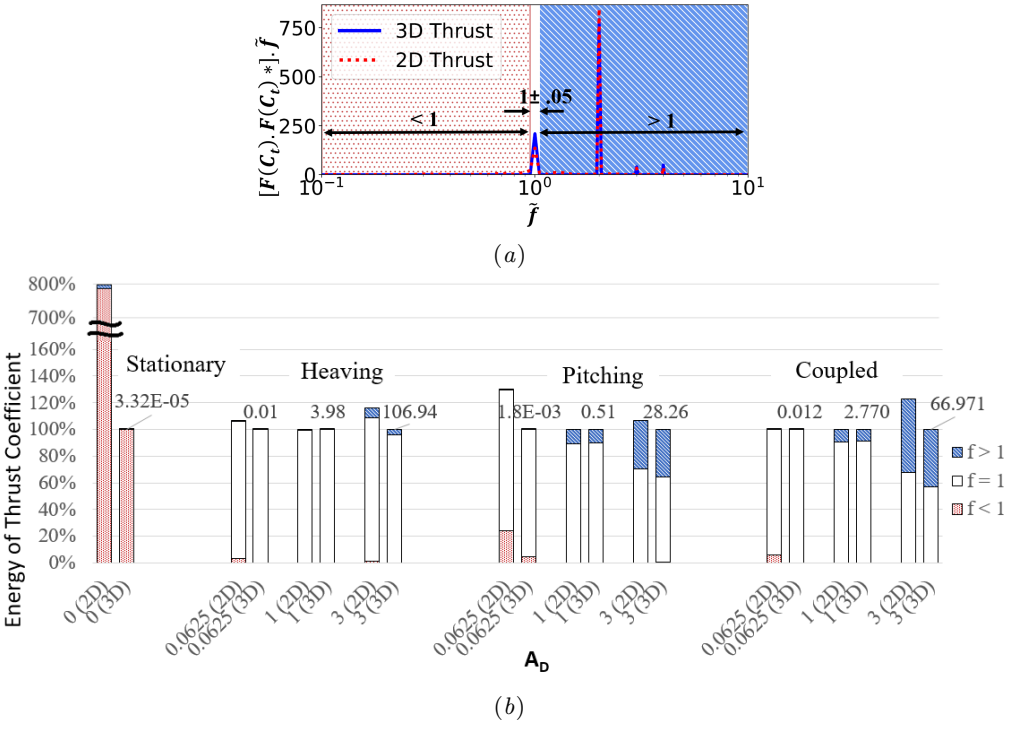

Figure 7: (*a*) Category division for C_t power spectra versus frequency (normalised to flapping frequency), and (*b*) C_t power-spectra integral or variance in percentage for 3 different $A_D s$. Each 3D-bar is scaled as 100% with its total variance on top, provided with the category divisions and accompanied by 2D on its left scaled as a percentage corresponding to the 3D.

It is seen that coupled and pitching motions have large contributions (over 20%) from $\tilde{f} > 1$ at high values of A_D. The relative contributions are small for heave motions, however, since the absolute value of fluctuations in heave motions are much higher than other kinematics (as seen by the numerical value at the top), the absolute value from $\tilde{f} > 1$ is very comparable across different kinematics. This suggests that there could be a universal mechanism that leads to higher frequency force fluctuations regardless of kinematics. This mechanism could be related to the breakdown of the leading-edge vortices along the spanwise direction. This is further explored below.

3.6. *Breakdown of LEVs*

The transition from 2D back to 3D with increasing A_D is expected to be due to spanwise instability that leads to the breakdown of the vortices. As they grow in strength, vortices burst and form non-uniform small structures along the span. This breakdown appears to be at different values of A_D for different kinematics. This can be examined by calculating the circulation of the leading-edge vortex for different values of A_D and different kinematics. Figure 8 shows the variation in the circulation of LEVs, now represented as a Reynolds number (with $Re = \Gamma/\nu$). This circulation is calculated as the integral of vorticity over a box as shown in the inset in figure 8. This box was chosen at a given phase where a vortex is just shed from the leading-edge separation bubble. Since the frequency of flapping is the same for all simulations, the location and size of this box

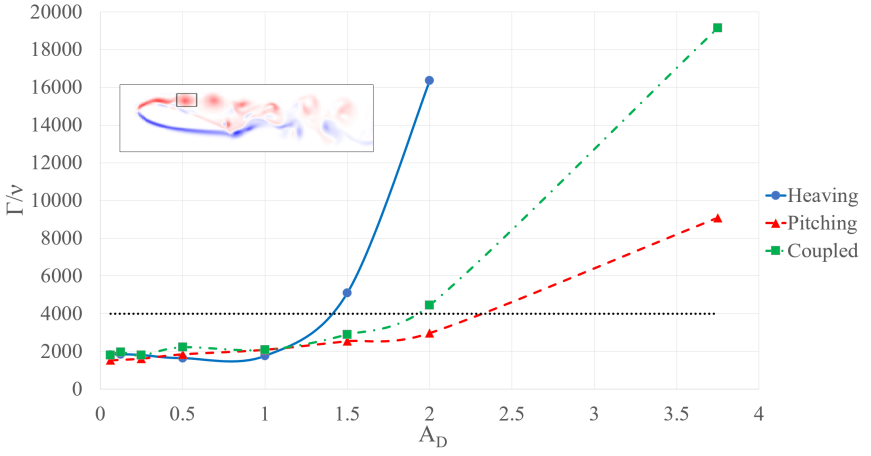

Figure 8: Evolution of leading-edge vortex circulation over kinematic viscosity along the increase of A_D. The flow above dotted black line show 3D structures.

did not have to change across the different kinematics. The sensitivity for box sizes and locations are provided in figure 9. Finally, a comparison of the circulation between 2D and 3D simulations did not reveal any noticeable difference before the vortices start to breakdown. This is because we are examining the "first" vortex that is shed, which are very similar regardless of the case.

The figure indicates that Reynolds numbers (or the circulation) of the LEVs appear to grow exponentially with increasing A_D. The rate of increase is different for different kinematics. The growth in heaving is the fastest among the three types of motion indicated why it has the shortest range of Strouhal numbers with 2D structures. In comparison, pitching and coupled motions have a more gradual growth leading to wider ranges for the presence of 2D structures. It should be noted that the coupled motion is dominated by pitching and therefore resembles the pitching kinematics.

The horizontal dotted black line in figure 8 indicates the circulation of the LEVs where uniforms 2D structures transition to 3D structures. The cases where the circulation of LEVs are higher than this value show vortex breakdown and smaller-scale structures accompanied by force fluctuations in higher frequencies. This is universally true regardless of the kinematics, This circulation or Reynolds number of LEVs, $\Gamma/\nu \approx 4000$ is the critical Reynolds number where the balance between vortex strength (induced by the kinematics) and viscous diffusion is lost leading to vortex breakdown. This critical Reynolds number is akin to the Reynolds number of a cylinder where there is a spanwise breakdown of vortices. However, for that case, the Reynolds number based on the cylinder diameter is much smaller than 4000. Regardless, the mechanism for the transition from 2D to 3D type flow structures appears to be similar.

4. Conclusion

This work demonstrates that spanwise-uniform 2D structures are discovered at intermediate St_A of flapping foil, while strong 3D structures are found at higher and lower St_A. These 3D structures are produced over the span without being initiated by tip effect. In the intermediate St_A region with spanwise-uniform (2D) structures, all statistics of force coefficients (lift and drag) such as mean, maximum and variance are similar between 2D and 3D simulations. These 2D structures are found at $St_A \approx 0.3$ in heaving motion,

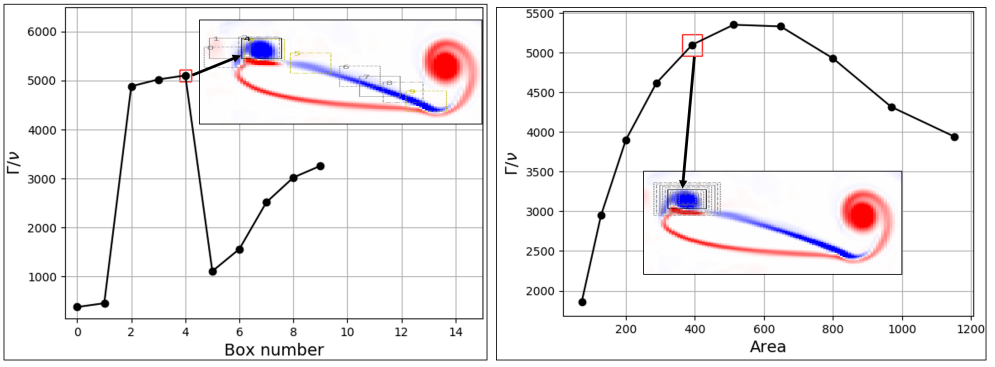

(a) (b)

Figure 9: Sensitivity analysis for (a) box locations and (b) box sizes. The highlighted box size and location were chosen for the study and the results are shown in figure 8.

$St_A \approx 0.3$–0.6 in pitching and $St_A \approx 0.15$–0.45 in coupled motion. Critically, the coupled motion gives a sufficient range for 2D structures to cover the optimal-efficiency St_A region for swimming animals mentioned by Triantafyllou *et al.* (1993), proving that 2D simulations are valid in this region.

In the regions where 3D vortex structures appear at higher and lower St_A, we discover discrepancy of mean force-coefficients between 2D and 3D simulations and over-prediction in 2D-simulation variances. The appearance of 3D structures at lower St_A is accompanied by more stable LEVs and discrepancies in the separation and recirculation areas. Meanwhile, the flow field of 2D simulation at higher St_A indicates non-dissipative vortices causing high force fluctuations and disturbance in the wake trajectories, LEVs and TEVs.

By analysing the variance of thrust-coefficient signals, we conclude that the transition from 3D to 2D vortex wake at intermediate St_A is due to the kinematics overwhelming the stationary foil's 3D drag wake. This is supported by the fact that the transition occurs at the same amplitude as the occurrence of reverse Bénard-von-Kármán propulsive wakes. Meanwhile, the 2D-to-3D transition from intermediate to higher St_A is due to high-energy LEVs overpowering the damping effect of viscosity causing the LEVs breakdown at $\Gamma/\nu \approx 4000$.

The application of strip theory may still be valid but only at the range of St_A where the flow structures are uniformly 2D. Outside of this, the validity is questionable signifying that the strip theory should not be applied at high St_A or low St_A. The 2D-structure window is found relatively wider in pitch-dominating motion. For manoeuvring and taking off flying, where heaving motion is significant and normally at higher St_A, 3D simulations are necessary regardless of the effect of tip vortices. In the future, this research will be continued using 3D shape (including tip effect) and 3D motion (rolling and twisting motions) to comprehensively study the application of strip theory to finite flapping foils.

Acknowledgement

We would like to thank Indonesia Endowment Fund for Education (LPDP) and IRIDIS High Performance Computing Facility with its associated support services at the University of Southampton for the completion of this work.

REFERENCES

Andersen, A., Bohr, T., Schnipper, T. & Walther, J. H. 2016 Wake structure and thrust generation of a flapping foil in two-dimensional flow. *Journal of Fluid Mechanics* **812**.

Carr, Z. R., Chen, C. & Ringuette, M. J. 2013 Finite-span rotating wings: three-dimensional vortex formation and variations with aspect ratio. *Experiments in Fluids* **54** (2).

Deng, J., Sun, L., Teng, L., Pan, D. & Shao, X. 2016 The correlation between wake transition and propulsive efficiency of a flapping foil: A numerical study. *Physics of Fluids* **28** (9), 094101.

Eloy, C. 2012 Optimal strouhal number for swimming animals. *Journal of Fluids and Structures* **30**, 205–218.

Fu, J., Hefler, C., Qiu, H. & Shyy, W. 2015 Effects of aspect ratio on flapping wing aerodynamics in animal flight. *Acta Mechanica Sinica* **30** (6), 776–786.

Garcia, B. F., Weymouth, G. D. & Tutty, O. R. 2017 Analysis of two-dimensional and three-dimensional wakes of long circular cylinders. *OCEANS 2017 - Aberdeen* .

Godoy-Diana, R., Aider, J. L. & Wesfreid, J. E. 2008 Transitions in the wake of a flapping foil. *Phys Rev E Stat Nonlin Soft Matter Phys* **77** (1 Pt 2), 016308.

Isogai, K., Shinmoto, Y. & Watanabe, Y. 1999 Effects of dynamic stall on propulsive efficiency and thrust of flapping airfoil. *AIAA Journal* **37** (10), 1145–1151.

Koochesfahani, M. M. 1989 Vortical patterns in the wake of an oscillating airfoil. *American Institute of Aeronautics and Astronautics* **27** (9), 1200–1205.

Lei, C., Cheng, L. & Kavanagh, K. 2001 Spanwise length effects on three-dimensional modelling of flow over a circular cylinder. *Computer Methods in Applied Mechanics and Engineering* **190**, 2909–2923.

Lentink, D. & Dickinson, M. H. 2009 Rotational accelerations stabilize leading edge vortices on revolving fly wings. *J Exp Biol* **212** (Pt 16), 2705–19.

Lu, Y., Shen, G. X. & Lai, G. J. 2006 Dual leading-edge vortices on flapping wings. *J Exp Biol* **209** (Pt 24), 5005–16.

Maertens, P. A. & Weymouth, G. D. 2014 Accurate cartesian-grid simulations of near-body flows at intermediate reynolds numbers. *Computer Methods in Applied Mechanics and Engineering* .

Mittal, R. & Balachandar, S. 1995 Effect of three-dimensionality on the lift and drag of nominally two-dimensional cylinders. *Physics of Fluids* **7** (8), 1841–1865.

Moriche, M., Flores, O. & García-Villalba, M. 2016 Three-dimensional instabilities in the wake of a flapping wing at low reynolds number. *International Journal of Heat and Fluid Flow* **62**, 44–55.

Muscutt, L. E., Weymouth, G. D. & Ganapathisubramani, B. 2017 Performance augmentation mechanism of in-line tandem flapping foils. *Journal of Fluid Mechanics* **827**, 484–505.

Rohr, J. J. & Fish, F. E. 2004 Strouhal numbers and optimization of swimming by odontocete cetaceans. *Journal of Experimental Biology* **207** (10), 1633–1642.

Schnipper, T., Andersen, A. & Bohr, T. 2009 Vortex wakes of a flapping foil. *Journal of Fluid Mechanics* **633**, 411.

Taira, K. & Colonius, T. I. M. 2009 Three-dimensional flows around low-aspect-ratio flat-plate wings at low reynolds numbers. *Journal of Fluid Mechanics* **623**, 187.

Triantafyllou, G. S., Triantafyllou, M. S. & GrosenBaugh, M. A. 1993 Optimal thrust development in oscillating foils with application to fish propulsion. *Journal of Fluids and Structures* (7), 205–224.

Triantafyllou, M. S., Techet, A. H. & Hover, F. S. 2004 Review of experimental work in biomimetic foils. *IEEE Journal of Oceanic Engineering* **29** (3), 585–594.

Triantafyllou, M. S., Triantafyllou, G. S. & Gopalkrishnan, R. 1991 Wake mechanics for thrust generation in oscillating foils. *Physics of Fluids A: Fluid Dynamics* **3** (12), 2835–2837.

Uddin, E., Naseem, M. A., Khalid, S. U., Mubashar, A. & Shah, S. R. 2017 Investigation of the flow around uncambered airfoils at 1000 reynolds number using computational fluid dynamics for micro air vehicles. *The 2017 World Congress on Advances in Structural Engineering and Mechanics* .

Wang, S., Zhou, Y., Alam, M. M. & Yang, H. 2014 Turbulent intensity and reynolds number effects on an airfoil at low reynolds numbers. *Physics of Fluids* **26** (11), 115107.

Weymouth, G. D. & Yue, Dick K. P. 2011 Boundary data immersion method for cartesian-grid simulations of fluid-body interaction problems. *Journal of Computational Physics* **230** (16), 6233–6247.

Williamson, C. H. K. 1996 Vortex dynamics in the cylinder wake. *Annual Review of Fluid Mechanics* **28**, 477–539.

Williamson, C. H. K. 2006 Three-dimensional wake transition. *Journal of Fluid Mechanics* **328** (-1), 345.

Zhang, Jun 2017 Footprints of a flapping wing. *Journal of Fluid Mechanics* **818**, 1–4.